

Preference of cluster isomers as a result of quantum delocalization: Potential energy surfaces and intermolecular vibrational states of $\text{Ne}\cdots\text{HBr}$, $\text{Ne}\cdots\text{HI}$, and $\text{HI}(\text{Ar})_n$ ($n=1-6$)

Petr Slavíček, Martina Roeselová, and Pavel Jungwirth^{a)}

J. Heyrovský Institute of Physical Chemistry, Academy of Sciences of the Czech Republic and Center for Complex Molecular Systems and Biomolecules, Dolejškova 3, 18223 Prague 8, Czech Republic

Burkhard Schmidt

Freie Universität Berlin, Department of Mathematics/Scientific Computing, Arnimallee 2-6, 14195 Berlin, Germany

(Received 23 August 2000; accepted 27 October 2000)

Intermolecular vibrational states are calculated for $\text{Ne}\cdots\text{HBr}$, $\text{Ne}\cdots\text{HI}$, and $\text{HI}(\text{Ar})_n$ ($n=1-6$) complexes using potential energy surfaces constructed by accurate *ab initio* methods. Potentials of rare gas–hydrogen halide clusters exhibit two collinear minima, one corresponding to hydrogen lying between the heavy atoms, and the other to hydrogen facing away from the rare gas atom. The relative depths of the two minima are a result of a subtle balance between polarization and dispersion interactions. Moreover, due to a large quantum delocalization in the hydrogen bending (librational) motion the relevance of a particular stationary point on the potential energy surface is only limited. It is more appropriate to discuss the isomers in terms of vibrationally averaged structures. For $\text{Ne}\cdots\text{HBr}$ the potential minimum and the vibrationally averaged structure correspond to the same isomer with hydrogen between neon and bromine. However, for $\text{Ne}\cdots\text{HI}$ the global minimum corresponds to the $\text{Ne}\cdots\text{IH}$ collinear geometry, while the vibrationally averaged structure has hydrogen between the heavy atoms. In the case of $\text{HI}(\text{Ar})_n$ we show that one can flip between the two isomers by adding argon atoms, which reconciles the seemingly contradictory experimental results obtained for the photodissociation of $\text{HI}\cdots\text{Ar}$ on one side, and of large $\text{HI}(\text{Ar})_n$ clusters on the other side. © 2001 American Institute of Physics. [DOI: 10.1063/1.1333705]

I. INTRODUCTION

Small hydrogen halide–rare gas clusters serve as prototypes of mixed weakly bound systems for studying intermolecular interactions. Considerable attention has been paid, both by theory and experiment, to the structure and interactions of systems with a single rare gas atom, i.e., of $\text{Rg}\cdots\text{HX}$ complexes, where Rg is most often neon or argon, and $\text{X}=\text{F}$, Cl , Br , or I .^{1–15} In all cases, the potential energy surface (PES) of the complex exhibits two distinct minima, one corresponding to the $\text{Rg}\cdots\text{HX}$ and the other to the $\text{Rg}\cdots\text{XH}$ isomer, separated by a relatively shallow barrier.^{7–12} The former structure, where the hydrogen lies between the heavy atoms, is stabilized primarily by polarization forces, since in this geometry the permanent dipole and quadrupole of the HX moiety induce an attractive electric response of the rare gas atom. On the other hand, for the latter isomer, where hydrogen points away from the rare gas atom, dispersion interaction between the heavy atoms dominates. This simple qualitative analysis allows to rationalize the fact, that hydrogen fluoride and chloride with a large ionic character prefer the $\text{Rg}\cdots\text{HX}$ isomer, while for hydrogen bromide and especially iodide, which are more covalently bound, dispersion interac-

tions are competitive enough, so that in some cases the $\text{Rg}\cdots\text{XH}$ structure actually becomes more stable.

The knowledge of the structure of $\text{Rg}\cdots\text{HX}$ complexes is not only interesting per se but it is also important in connection with the cage effect¹⁶ in clusters. The cage effect, which is the ability of the environment to hinder the photodissociating solute molecule, has been investigated in great detail in hydrogen halide–rare gas clusters.^{17–30} Although a single Rg atom is rather inefficient in hindering the photolyzed highly energetic hydrogen, in larger rare gas clusters caging becomes much more important. It has been shown recently, that the efficiency of caging depends not only on the cluster size, but also on the position of the HX impurity (embedded vs surface), and, especially for the surface structures, on the particular initial orientation of the hydrogen atom.^{25,30}

A necessary condition for understanding the vibrational dynamics and for interpreting the spectra of the $\text{Rg}\cdots\text{HX}$ complexes is a construction of an accurate PES. This is achieved either by inverting experimental data obtained by high resolution vibrational/rotational spectroscopy, or by state-of-the-art quantum chemical calculations. Recently, attempts have been made to merge the two approaches, and a precalculated PES has been improved via a “morphing” procedure using spectroscopic data.⁵ Currently, high quality potentials exist for $\text{Ar}\cdots\text{HF}$, $\text{Ar}\cdots\text{HCl}$, $\text{Ar}\cdots\text{HBr}$, $\text{Ar}\cdots\text{HI}$, and $\text{Ne}\cdots\text{HCl}$ complexes.^{5,7–12} In this paper, we provide

^{a)}Author to whom correspondence should be addressed. Electronic mail: jungwirth@jh-inst.cas.cz.

hitherto uninvestigated PESs of the $\text{Ne}\cdots\text{HBr}$ and $\text{Ne}\cdots\text{HI}$ complexes, important for the interpretation of recent photodissociation cluster experiments.^{31,32}

An interesting feature of hydrogen halide–rare gas clusters is connected with the fact that they are typically prepared via supersonic expansion into the vacuum through a narrow nozzle.³³ This technique leads to a very efficient cooling of the nascent clusters to temperatures ranging between several and several tens of Kelvins. Under these cryogenic conditions quantum vibrational effects cannot be neglected. This is particularly true for the cold and light hydrogen atom, which moves in a shallow intermolecular bending potential exhibiting a large amplitude bending (librational) motion.^{7,34} Due to this librational hydrogen delocalization, and partly also due to the soft intermolecular stretch (which actually couples to a certain extent with the hydrogen bend) the physical relevance of a particular point, minimum or saddle, on the PES of a $\text{Rg}\cdots\text{HX}$ complex is strongly limited. One should rather think in terms of vibrationally averaged structures, where the quantum effect of delocalization due to zero point motions is properly taken into account. In the present study, we demonstrate this issue on several examples, including an extreme case, where the vibrationally averaged structure corresponds to an isomer different from the global minimum on the PES. In this connection, note that the flip of isomers upon inclusion of zero point energy is not limited to $\text{Rg}\cdots\text{HX}$ systems. As has been shown recently, this effect is also found e.g., for the energetically lowest isomers of water hexamer.³⁵ In addition we demonstrate, that in the case of $\text{HI}(\text{Ar})_n$ ($n = 1-6$) one can actually flip between the isomer with the hydrogen pointing away from the cluster and that with hydrogen between the heavy atoms by simply adding argon atoms. We show that this finding reconciles seemingly contradictory experimental results on small vs large clusters.^{31,32,36}

The rest of the paper is organized as follows: System and geometry are briefly described in Sec. II, and Sec. III provides the computational details. Results and discussion are presented in Sec. IV. Finally, Sec. V contains concluding remarks.

II. SYSTEMS AND GEOMETRY

In this paper, we present *ab initio* potential energy surfaces and calculations of intermolecular vibrational states of $\text{Ne}\cdots\text{HI}$ and $\text{Ne}\cdots\text{HBr}$ van der Waals complexes. Librational calculations have also been performed for $\text{HI}(\text{Ar})_n$ ($n = 1-6$) clusters. For the calculation of vibrational states of $\text{Rg}\cdots\text{HX}$ clusters we used the standard Jacobi coordinates. R is the distance between the rare gas atom and center of mass of hydrogen halide molecule, r is the internuclear distance for the HX molecule, and Θ is the angle between vectors \mathbf{R} and \mathbf{r} . These coordinates are depicted in Fig. 1. For the *ab initio* calculations we used slightly different coordinates, with R being the distance between the halogen atom and the rare gas atom. Since the centers of mass of both HBr and HI practically coincide with the halogen atoms, for all practical purposes the difference between the two coordinate sets can be neglected. Finally, the black dot in Fig. 1 marks the localization of the bonding basis functions (see Sec. III).

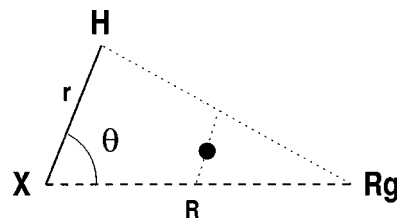


FIG. 1. Geometry and Jacobi coordinates (r, R, Θ) of the $\text{Rg}\cdots\text{HX}$ complex. The filled circle halfway between the $\text{Rg}-\text{X}$ and $\text{Rg}-\text{H}$ midpoints indicates the position of the bond functions used in the *ab initio* calculations.

III. COMPUTATIONAL DETAILS

A. *Ab initio* method

It is well known that for the $\text{Rg}\cdots\text{HX}$ complexes the dispersion energy is an important part of interaction energy. Therefore, for an adequate description of such systems, it is imperative to include a dominant part of electron correlation. In the calculations reported here, we have used coupled clusters CCSD(T) method and, for comparison, also the second order Møller–Plesset perturbation theory (MP2). Due to their size extensivity both MP2 and CCSD(T) methods are appropriate for intermolecular energy calculations.

We have calculated the intermolecular energy within the supermolecular approach, in which the interaction energy is given as a difference between the total energy of the complex (E_{RgHX}) and the sum of the energies of the subsystems ($E_{\text{HX}} + E_{\text{Rg}}$). Within this approach, removal of basis set superposition error (BSSE) is absolutely necessary. We have, therefore, applied the standard counterpoise method (CP),³⁷ including both atom centered and bond basis functions.

The quality of intermolecular energy calculations for weakly bound systems strongly depends on the choice of the electronic basis. The employed basis set, presented in detail in Table I, has an atom centered and bond region centered parts. The latter part is common for all complexes under investigation. The atom centered basis functions for H, Ar, Br, and Cl correspond to the aug-cc-pVDZ basis set.³⁸ These standard basis sets have been augmented by one function of d symmetry (for hydrogen), or of f symmetry (for chlorine, argon and bromine), with exponents of 0.15 (H), 0.23 (Ar), 0.15 (Cl), and 0.25 (Br).^{39–43} All these exponents were optimized with respect to the dispersion term.⁴³ For neon we have used the augmented double- ζ ANO basis set.⁴² While for $\text{Rg}\cdots\text{HX}$ complexes with $\text{X}=\text{Cl}$ or Br the calculations include all electrons, for systems with iodine we have used

TABLE I. Basis sets and contraction schemes used in the *ab initio* calculations.

Location	Basis set
H	(5s2p1d)/[3s2p]
Cl	(13s9p2d1f)/[5s4p2d1f]
Br	(15s12p7d1f)/[16s5p3d]
I	AREP+(7s5p4d1f)
Ne	(14s9p4d)/[4s3p2d]
Ar	(13s9p2d1f)/[5s4p2d1f]
Midbond region	3s(0.9,0.3,0.1),3p(0.9,0.3,0.1), 2d(0.6,0.2)

an average relativistic effective potential (AREP).⁴⁴ We have modified the iodine valence double- ζ basis proposed in this work in the same way as described in Refs. 45 and 46 by adding one polarization d function with an exponent of 0.28 and s and p diffuse functions with exponents of 0.033 35 and 0.045 36. For Ar \cdots HI test calculation we have used also a correlation consistent polarized triple- ζ basis set.⁴⁵ This basis set has served originally for relativistic all electron calculation, therefore, we have modified it in a similar way as in Ref. 47. Namely, we have neglected the core atomic orbitals and we have assumed only the large component basis.

It has been demonstrated in Refs. 48–51 that adding a small number of basis functions to the midbond region is a very efficient way for improving the description of dispersion energy. Whereas the location of such basis functions for atom–atom systems is straightforward,⁴⁸ the situation for anisotropic systems is more ambiguous. Fortunately, the results are not very sensitive to the exact location of these functions in the intermolecular bond region.⁵⁰ We have found that a balanced description is achieved when the bonding functions are placed in the middle of the abscissa given by midpoints of Rg–X and Rg–H bonds (see Fig. 1). This bond basis consists of the three s functions (exponents of 0.9, 0.3, and 0.1), three p functions (exponents of 0.9, 0.3, and 0.1) and two d functions (exponents of 0.6 and 0.2). This set has been successfully applied to rare gas dimers⁴⁸ and to various anisotropic systems, such as Ar \cdots HF, Ar \cdots H₂O, and Ar \cdots NH₃.⁴⁹ According to these studies, the interaction energies are rather insensitive to the change of the orbital exponents and the set should be broadly applicable to different intermolecular systems.

All *ab initio* calculations reported in this paper have been performed using the GAUSSIAN 98 program package.⁵²

B. Calculation of vibrational states

The bound states of Ne \cdots HBr and Ne \cdots HI complexes were calculated using the coupled channel scheme in which the total wave function is expanded in terms of rotational functions of the HX molecule. We used an exact Hamiltonian for an atom–(rigid) diatom system expressed in standard Jacobi coordinates (see Fig. 1),

$$\hat{H} = -\frac{\hbar^2}{2\mu_1} \left(\frac{1}{R} \frac{\partial^2}{\partial R^2} R - \frac{\hat{l}^2}{\hbar^2 R^2} \right) + \frac{\hat{j}^2}{2\mu_2 r^2} + V(R, \Theta), \quad (1)$$

where $\mu_1 = M_{\text{Rg}} M_{\text{HX}} / (M_{\text{Rg}} + M_{\text{HX}})$ is the reduced mass of the Rg \cdots HX complex, μ_2 is the reduced mass of the HX molecule, \hat{l} is the angular momentum operator for end-over-end rotation of the complex (i.e., corresponding to the R coordinate), and \hat{j} is the angular momentum of the internal rotation of HX, which is assumed to be a rigid rotor with the internuclear distance r fixed to its equilibrium value. Finally, $V(R, \Theta)$ is the intermolecular potential for interaction of a HX molecule with a rare gas atom.

In this study, we have assumed that the total angular momentum $\hat{J} = \hat{j} + \hat{l}$ is equal to zero. This leads to a significant reduction of the number of coupled states (and thus the number of the coupled equations to be solved), and also to simplification of the Hamiltonian since then $\hat{l}^2 = \hat{j}^2$. The total

wave function can be then expanded in spherical harmonics $Y_{j0}(\Theta)$ of the $C_{\infty v}$ point group describing the angular degrees of freedom corresponding to the internal rotation of the HX molecule

$$\Psi(R, \Theta) = \frac{1}{R} \sum \chi_{j0}(R) Y_{j0}(\Theta). \quad (2)$$

Substitution of the above expansion into the total Schrödinger equation with the Hamiltonian given by Eq. (1) yields a set of coupled equations for the radial functions $\chi_{j0}(R, t)$,

$$i\hbar \frac{\partial}{\partial t} \chi_{j0}(R, t) = \left[-\frac{\hbar^2}{2\mu_1} \frac{\partial^2}{\partial R^2} + \left(\frac{\hbar^2}{2\mu_1 R^2} + \frac{\hbar^2}{2\mu_2 r^2} \right) j(j+1) \right] \times \chi_{j0}(R, t) + \sum_{j'} \chi_{j'0}(R, t) V_{jj'}, \quad (3)$$

where the potential matrix is defined by $V_{jj'} = \langle j'0 | V(R, \Theta) | j0 \rangle$. The radial wave function is represented on a spatial grid of 256 equidistant points. We solved this set of equations using the imaginary time propagation scheme,⁵³ where the Chebyshev propagator with a time step of $\tau = 25$ fs was employed. We truncated the expansion into spherical harmonics at $j_{\text{max}} = 7$, which leads to fully converged results. Typically, 100 time steps are required to fulfill the criterium $\langle \Psi(t+\tau) | \Psi(t) \rangle > 1 - 1 \times 10^{-7}$. Vibrationally excited states were also obtained by imaginary time propagation, where at each evaluation of the Hamiltonian the contribution of lower states is projected out. For the systems under study, all bound states can be reliably obtained in this way.⁵³

For the construction of vibrational states of larger clusters with more than one rare gas atom, it is not computationally feasible to perform the calculations in full dimensionality. Therefore, we have used a partially separable approach, analogous to that used in our previous studies.^{29,30} Briefly, the total wave function is expressed as

$$\Psi(q_1, q_2, \dots, q_{3n-6}, \Theta, \Phi) = \phi_1(q_1) \cdots \phi_{3n-6}(q_{3n-6}) \phi_{\text{lib}}(\Theta, \Phi, \{q_{ij}\}), \quad (4)$$

where q_i are the normal coordinates of the cage (i.e., heavy atoms). The cage modes are taken into account within the harmonic approximation, while the librational wave function of the HX molecule $\phi_{\text{lib}}(\Theta, \Phi)$ is calculated by diagonalization of the HX (hindered) rotational Hamiltonian in the basis of spherical harmonics, i.e., we assume only the last two terms on the right-hand side of Eq. (1),

$$\hat{H} = \frac{\hat{j}^2}{2\mu_2 r^2} + V(\Theta, \Phi, \{q_{ij}\}). \quad (5)$$

The term connected with the overall rotation of the cluster is neglected since $\mu_1 R^2$ is much larger than $\mu_2 r^2$. Due to the loss of cylindrical symmetry the potential V is in such cases also Φ -dependent. Finally, both the potential for the hindered rotation of HX and the librational wave functions are parametrically dependent on the cage coordinates.

This approach is satisfactory for systems, where the minima corresponding to HX–Rg_n and XH–Rg_n structures are well separated or correspond to similar heavy atom ge-

TABLE II. Results of test calculations at the CCSD(T) level. The table compares the global and secondary minima of the PES for four different Rg··HX complexes with the results of previous studies.

System	Θ°	CCSD(T) calculation/ cm^{-1}	MP2 calculation/ cm^{-1}	Previous value/ cm^{-1}	Reference
Ar··HCl	0	-173	-191	-175	7
Ar··HCl	180	-141	-161	-139	7
Ar··HBr	0	-168	-190	-165	12
Ar··HBr	180	-158	-181	-160	12
Ne··HCl	0	-66	-59	-68	8
Ne··HCl	180	-52	-48	-53	8
Ar··HI	180	-185	-215	-220	5
Ar··HI	0	-148	-174	-173	5

ometries and, therefore, we can separate the bending and stretching modes. The energy gap between minima corresponding to possible isomeric structures is increasing with the number of rare gas atoms. As will be discussed in detail in the Sec. IV B calculations in full dimensionality for the case of the smallest HX–Rg clusters indicate that the approximate approach is reasonable, in particular for the ground state wave function. Thus, the coupling between vibration and internal rotation does not have a strong effect on the ground state structure of the explored complexes (Ar··HI and Ne··HI), however it can seriously influence the excited bound state.

IV. RESULTS AND DISCUSSION

A. Test calculations

In order to confirm the reliability of the employed *ab initio* method and basis sets, we have performed test calculations on Rg··HX systems for which good empirical or semiempirical potentials are available. Thus, we have first reinvestigated Ar··HCl, Ne··HCl, Ar··HBr, and Ar··HI complexes. We have calculated the interaction energies both at MP2 and CCSD(T) levels. The results of our calculations are listed in Table II.

The agreement between experimental potentials and calculated *ab initio* values is strikingly good. For Ar··HCl, the global minimum lies 175 cm^{-1} under the dissociation limit,⁷ while the calculated value at the CCSD(T) level is -173 cm^{-1} . For the secondary minimum values of -139 cm^{-1} and -141 cm^{-1} are the experimental and calculated dissociation energies. Similarly, the experimental dissociation energies for the global and the secondary minimum of the Ar··HBr complex are -165 and -160 cm^{-1} ,¹² while the present calculations give -168 and -158 cm^{-1} . Also for Ne··HCl cluster our calculations are very close to experimental values:⁸ -68 vs -66 cm^{-1} for the global minimum and -53 vs -52 cm^{-1} for the secondary minimum. The MP2 interaction energies are close to the CCSD(T) values for Ne··HCl, while MP2 overestimates the binding energy by approximately 20 cm^{-1} for Ar··HBr and Ar··HCl. However, the difference in energies between the global and the secondary minima are very similar for the MP2 and CCSD(T) calculations and for empirical potentials.

For the Ar··HI complex, we have calculated the energy of the global minimum to be -185 cm^{-1} at the CCSD(T) level, while the recently published semiempirical potential gives of -220 cm^{-1} , the values for secondary minimum being -148 and -172.7 cm^{-1} , respectively. The agreement is satisfactory and our calculations reproduce also the shape of the semiempirical potential and provide the correct order of the global and the secondary minima. Note also, that the MP2 energies are shifted by 30 cm^{-1} and are very close to the semiempirical potential (which is actually based on MP2 calculations). We stress already here that the difference between MP2 and CCSD(T) is much smaller for Ne··HI than for the Ar··HBr and Ar··HCl complexes. We have also tested a larger iodine basis set of a triple- ζ quality, yielding the CCSD(T) global and secondary minima of -193 and -149 cm^{-1} , which is very close to the results obtained with the double- ζ quality basis set. Note also that our calculated value of the dissociation energy corrected for zero point vibrations would lie between the value of -93 cm^{-1} given by Heaven⁵⁴ on the basis of HI–Ar photodissociation experiment and the value of -146.4 cm^{-1} based on the semiempirical potential of Bevan *et al.*⁵

B. Potential energy surfaces of Ne··HBr and Ne··HI

We have calculated *ab initio* interaction energies on an R and Θ grid, constraining the H–X bond distance to its equilibrium value of 1.414 \AA for HBr and 1.609 \AA for HI. The HX–Rg angle Θ has been varied from 0 to 180° with a 30° step and the X–Rg coordinate R has been varied from 3.2 \AA to 6.0 \AA with a step of 0.1 \AA around the minima and 0.5 \AA elsewhere. All energies have been calculated at the CCSD(T) level, except for repulsive geometries with highly positive energies, where MP2 energies practically coincide with the CCSD(T) energies and the MP2 description, therefore, suffices. Thus, we have represented the Ne··HBr and Ne··HI interaction potential by approximately 90 points calculated at the CCSD(T) level. The potential was then interpolated by cubic splines. The Ne··HBr PES is depicted in Fig. 2, and the Ne··HI potential is depicted in Fig. 3. These figures have been produced using the CCSD(T) interaction energies, however, MP2 interaction energies are typically only 2 – 3 cm^{-1} above those obtained using the CCSD(T) method. This correspondence implies that the results are converging well with respect to recovering the correlation energy.

The general features of the Ne··HI and Ne··HBr PESs are similar to those of analogous Rg··HX complexes. Namely, these potential functions are characterized by two minima, and both the global and secondary minima correspond to collinear geometries. Important characteristics of the potentials such as geometries and energies of the global minimum, secondary minimum, and the barrier between them are listed in Table III. The global minimum of the Ne··HBr complex lies 58.6 cm^{-1} below the dissociation limit. The $\Theta=0^\circ$ value for this minimum corresponds to neon facing the hydrogen with $R_m=4.07 \text{ \AA}$. The secondary minimum is energetically very close to the global minimum: energy of -55.7 cm^{-1} at $\Theta=180^\circ$ (neon is on the other side of the halogen atom than hydrogen), and $R_m=3.55 \text{ \AA}$. The two minima are practically isoenergetic, however, as will be

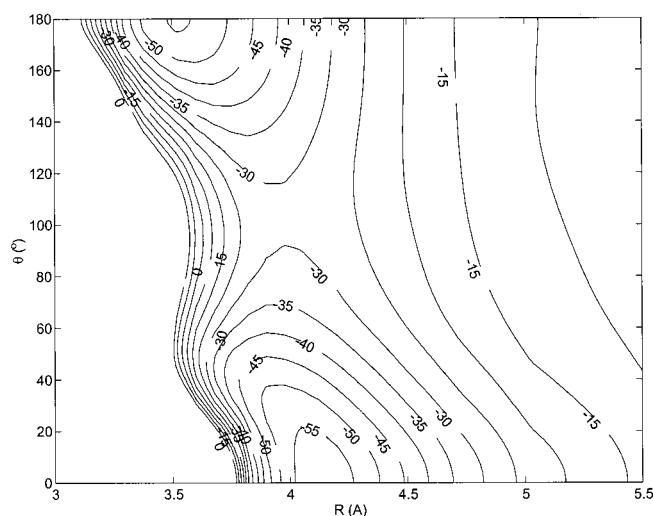


FIG. 2. Potential energy surface of the $\text{Ne}\cdots\text{HBr}$ complex in the (R, Θ) plane obtained by CCSD(T) calculations. The contour labels give the interaction energy in cm^{-1} . Note that a value of $\Theta = 0^\circ$ corresponds to the $\text{Ne}\text{-HBr}$ geometry, while $\Theta = 180^\circ$ corresponds to the $\text{Ne}\text{-BrH}$ arrangement.

discussed in the next section, the zero point energy clearly prefers the former structure. The transition state between these two minima has an energy of -30.5 cm^{-1} at $\Theta = 90^\circ$ and $R_m = 4.00 \text{ \AA}$. Another important feature of this PES is its anisotropy. The value of the optimal distance R_m for a given Θ continuously decreases with increasing Θ .

For the $\text{Ne}\cdots\text{HI}$ complex, the global minimum corresponds to neon on the other side of the halogen atom than hydrogen ($\Theta = 180^\circ$, $R_m = 3.75 \text{ \AA}$). The energy of this point on the potential energy surface is -55.7 cm^{-1} . The secondary minimum (for $\Theta = 0^\circ$) lies 7.6 cm^{-1} above the global minimum and its corresponding intermolecular distance R is 4.48 \AA . The transition state is characterized by $R_m = 4.3 \text{ \AA}$ and $\Theta = 90^\circ$ and the height of the barrier is 28.5 cm^{-1} .

As one can see from Figs. 2 and 3, both for the $\text{Ne}\cdots\text{HBr}$ and $\text{Ne}\cdots\text{HI}$ complexes the binding energy is small and potentials are rather flat. Note, that for such systems one should be careful with identifying the equilibrium structure of the

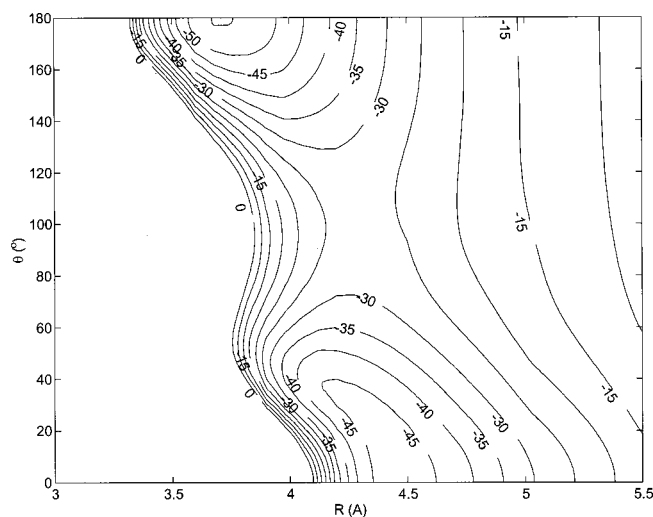


FIG. 3. Same as Fig. 2 but for the $\text{Ne}\cdots\text{HI}$ complex.

TABLE III. Results of calculations at the CCSD(T) level for the global and secondary minima, as well as the barrier (saddle) separating them, for $\text{Ne}\cdots\text{HBr}$ and $\text{Ne}\cdots\text{HI}$ complexes.

	$\text{Ne}\cdots\text{HBr}$	$\text{Ne}\cdots\text{HI}$
$\epsilon(0^\circ)/\text{cm}^{-1}$	-58.6	-48.1
$\epsilon(90^\circ)/\text{cm}^{-1}$	-30.5	-28.5
$\epsilon(180^\circ)/\text{cm}^{-1}$	-55.7	-55.7
$R_m(0^\circ)/\text{\AA}$	4.07	4.48
$R_m(90^\circ)/\text{\AA}$	4.00	4.30
$R_m(180^\circ)/\text{\AA}$	3.55	3.75

molecular system with the global minimum on the PES. Instead, the concept of vibrationally averaged structures, which takes into account the effect of zero point motions, should be employed.

The shape of the $\text{Ne}\cdots\text{HBr}$ and $\text{Ne}\cdots\text{HI}$ PESs is similar to those of the other members of the homologous series $\text{Rg}\cdots\text{HX}$ ($\text{Rg} = \text{Ne, Ar}$; $\text{X} = \text{F, Cl, Br, and I}$). The quantitative differences can be well understood in terms of the competition between dispersion and polarization interactions. While polarization prefers $\text{Rg}\text{-HX}$ isomers, dispersion favors the $\text{HX}\text{-Rg}$ geometries. Therefore, lighter halogens with a larger HX dipole have the former structure as a global minimum, while the latter arrangement is optimal for the $\text{Ar}\cdots\text{IH}$ complex. Finally, the polarizability of neon is much smaller than that of argon, which results in smaller interaction energies.

Quantitatively taking into account polarization and dispersion interaction, we obtain for the $E_{\text{Ne-HX}}/E_{\text{Ar-HX}}$ energy ratio the following expression:⁵⁵

$$\frac{E_{\text{Ne-HX}}}{E_{\text{Ar-HX}}} = \frac{\alpha_{\text{Ne}}}{\alpha_{\text{Ar}}} \left(\frac{r_{\text{Ar}}}{r_{\text{Ne}}} \right)^6 \frac{aI'_{\text{Ne}} + m}{aI'_{\text{Ar}} + m}, \quad (6)$$

where $I'_{\text{Rg}} = I_{\text{Rg}} I_{\text{HX}} / (I_{\text{Rg}} + I_{\text{HX}})$, $a = (2/3)\alpha_{\text{HX}}$, and $m = 4\mu_{\text{HX}}^2 / 4\pi\epsilon_0$. I is the ionization potential, μ is the dipole moment, and α is the polarizability. Taking $\text{Ar}\cdots\text{HBr}$ and $\text{Ar}\cdots\text{HI}$ semiempirical potentials as an existing reference, we obtain the global and secondary minima at -58 and -53 cm^{-1} for $\text{Ne}\cdots\text{HBr}$ and at -62 and -49 cm^{-1} for $\text{Ne}\cdots\text{HI}$. These estimated numbers are in a good agreement with our calculated *ab initio* interaction energies. We conclude by noting that further improvement of our potentials using the ‘‘morphing’’ approach¹⁰ would be possible when albeit limited experimental information on systems under study becomes available.

C. Bound states

One of the goals of this work is to explore the structure of the $\text{Ne}\cdots\text{HI}$ and $\text{Ne}\cdots\text{HBr}$ complexes in their ground states. With the knowledge of the potential energy surfaces of these complexes one can expect the large amplitude motion of the hydrogen atom to have a significant effect even in the ground state. Therefore, the usual concept of the structure as a geometry corresponding to the minimum on PES could be inadequate.

Vibrational wave functions of the bound states of the $\text{Ne}\cdots\text{HI}$ complex are depicted in Figs. 4, 5, and 6. Wave functions for the $\text{Ne}\cdots\text{HBr}$ cluster look similar, therefore we

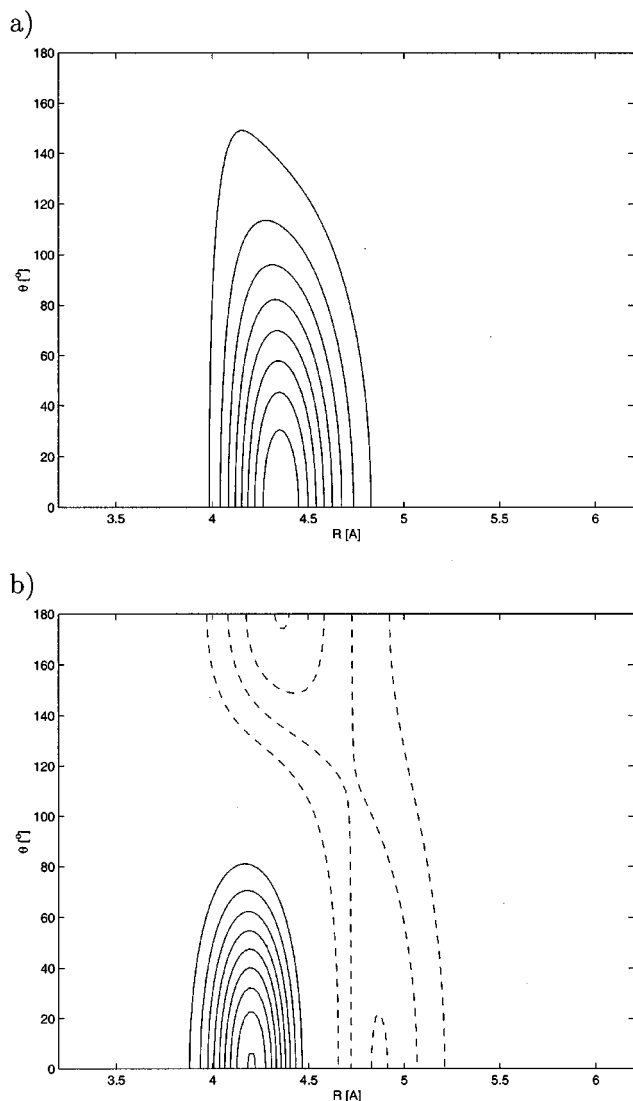


FIG. 4. Vibration densities (squared moduli of the wave functions) for the $\text{Ne}\cdots\text{HI}$ complex corresponding to a $\text{Ne}\text{--}\text{HI}$ vibrationally averaged structure (Σ^+ symmetry). (a) Vibrational ground state ($\epsilon = -28.3\text{ cm}^{-1}$). (b) Second vibrationally excited state ($\epsilon = -16.1\text{ cm}^{-1}$). Full line corresponds to positive and dashed line to negative sign of the corresponding vibrational wave function.

do not present them here. Figure 4(a) shows a contour plot of the square of the ground state wave function of the $\text{Ne}\cdots\text{HI}$ complex in R and Θ coordinates. Note that because the ground state wave functions are of Σ^+ symmetry, there is no Φ dependence. These wave functions have maximum at $\Theta = 0^\circ$ both for $\text{Ne}\cdots\text{HBr}$ and $\text{Ne}\cdots\text{HI}$. If we adopt the concept of vibrationally averaged structures, then such wave functions correspond to hydrogen pointing towards the neon. This is not surprising in the $\text{Ne}\cdots\text{HBr}$ case where this structure is also the minimum on the PES. On the other hand, the minimum on the $\text{Ne}\cdots\text{HI}$ PES corresponds to the $\text{Ne}\text{--}\text{IH}$ collinear structure (i.e., $\Theta = 180^\circ$). In this case, the structure is determined primarily by the quantum zero point motion connected with the shape of the potential, namely by the large amplitude motion of hydrogen atom in the angular coordinate. The value of the vibrationally corrected binding energy D_0 is -29.0 cm^{-1} for $\text{Ne}\cdots\text{HBr}$ and -28.3 cm^{-1} for

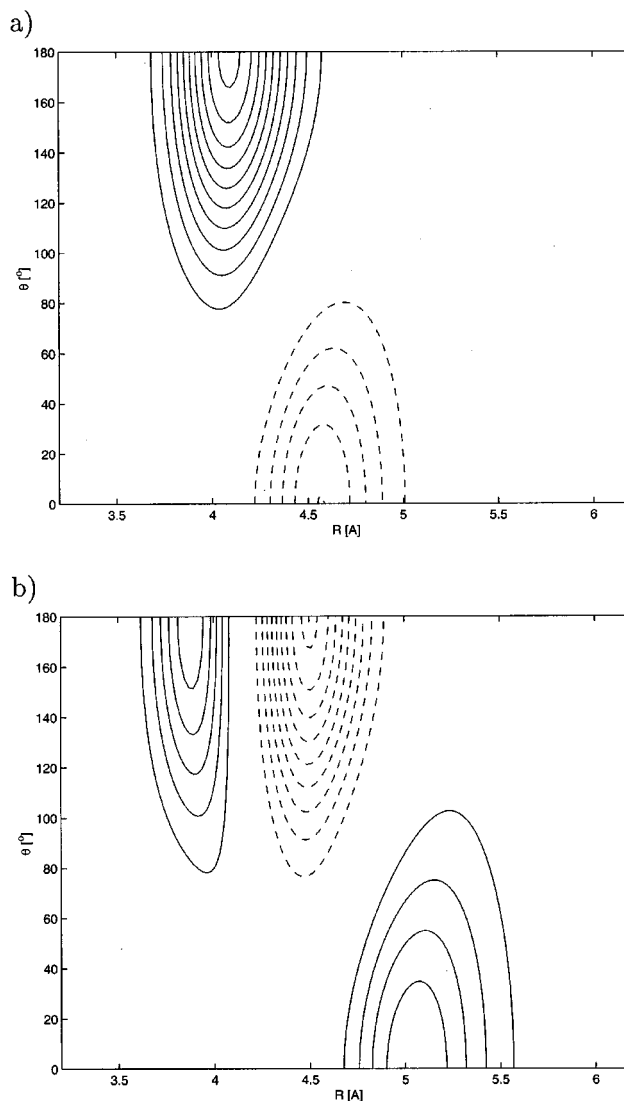


FIG. 5. Vibration densities (squared moduli of the wave functions) for the $\text{Ne}\cdots\text{HI}$ complex corresponding to a $\text{Ne}\text{--}\text{IH}$ vibrationally averaged structure (Σ^+ symmetry). (a) First vibrationally excited state ($\epsilon = -19.4\text{ cm}^{-1}$). (b) Fourth vibrationally excited state ($\epsilon = -9.7\text{ cm}^{-1}$). Full line corresponds to positive and dashed line to negative sign of the corresponding vibrational wave function.

$\text{Ne}\cdots\text{HI}$, the average R being 4.1 \AA and 4.3 \AA , respectively. For the $\text{Ne}\cdots\text{HI}$ case, this distance is significantly larger than that for the absolute minimum ($R = 3.75\text{ \AA}$). The wave function for $\text{Ne}\cdots\text{HBr}$ is similar in shape (the difference in R is given by different HX bond length for HBr and HI), and very close in energy. Note at this point that the electronic binding energy D_e for the $\text{Ne}\text{--}\text{HBr}$ isomer is -58.6 cm^{-1} , while only -48.1 cm^{-1} for the $\text{Ne}\text{--}\text{HI}$ isomer. However, since the rotational constant B is larger for HBr (8.473 cm^{-1}) (Ref. 56) than for HI (6.342 cm^{-1}),⁵ the differences in potential energy and in the rotational constants partly cancel each other. The discrepancy between geometries corresponding to the global minimum on the PES and to the vibrationally averaged geometry pertains also for the $\text{Ne}\cdots\text{DI}$ complex. The wave function (not shown here) is even more localized in the $\text{Ne}\cdots\text{DI}$ bending motion. It is clearly seen from Fig. 4(a) that the wave function of the ground state is well separable in R

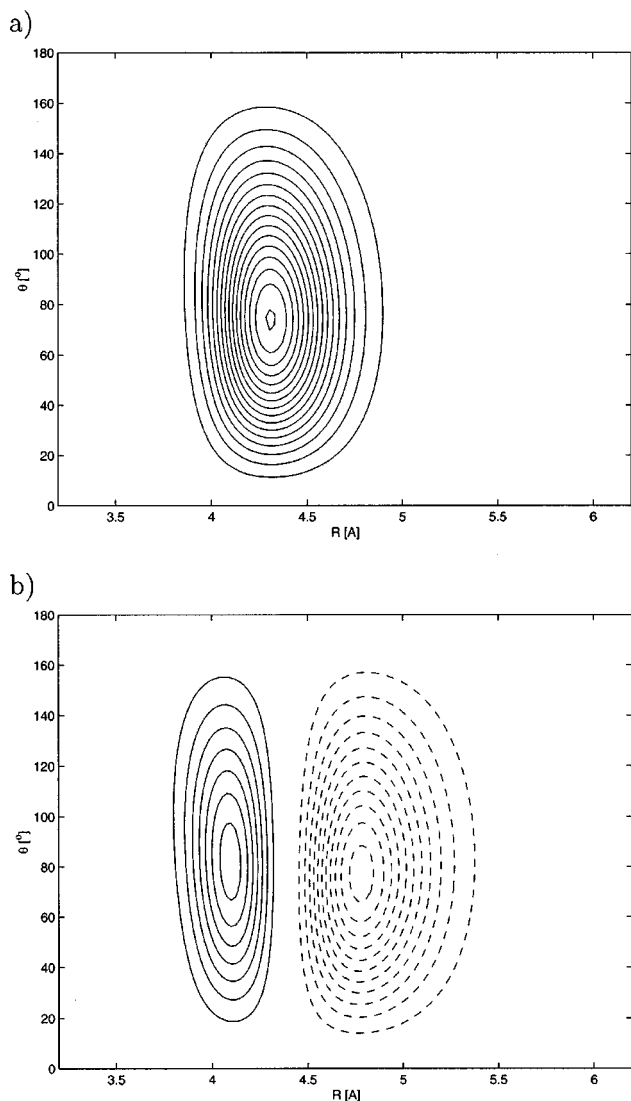


FIG. 6. Vibrational densities (squared moduli of the wave functions) for the $\text{Ne}\cdots\text{HI}$ complex corresponding to a T-shaped vibrationally averaged structure (Π symmetry). (a) Third vibrationally excited state ($\epsilon = -12.4 \text{ cm}^{-1}$). (b) Fifth vibrationally excited state ($\epsilon = -2.3 \text{ cm}^{-1}$). Full line corresponds to positive and dashed line to negative sign of the corresponding vibrational wave function.

and Θ . This provides further justification of the approximations used for larger clusters based on the bend/stretch separation.

Another interesting question is whether we can change the structure by vibrational excitation, i.e., whether we can identify some of the excited states with the second isomer. We have, therefore, calculated several low-lying bound states of the systems under investigation. The calculated energies of the lowest states are listed in Table IV. It can be generally said that the interpretation of the excited bound states in the sense of the second isomer is not straightforward. Figures 4 and 5 show the squares of the moduli of the wave functions of bound states of Σ^+ symmetry. The first state is the above discussed ground state (-28.3 cm^{-1}) corresponding to the $\text{Ne}-\text{HI}$ structure [Fig. 4(a)], while Fig. 4(b) depicts an excitation of $\text{Ne}\cdots\text{HI}$ complex with energy -16.1 cm^{-1} , which is the third state of Σ^+ symmetry. This

TABLE IV. Energies of the lowest bound intermolecular vibrational states of $\text{Ne}\cdots\text{HBr}$ and $\text{Ne}\cdots\text{HI}$ complexes in cm^{-1} .

Symmetry	$\text{Ne}\cdots\text{HBr}$	$\text{Ne}\cdots\text{HI}$
Σ^+	-29.0	-28.3
Σ^+	-15.6	-19.4
Σ^+	-12.9	-16.1
Σ^+	-5.4	-9.7
Π	-8.4	-12.4
Π		-2.3

excitation is predominantly of a stretching character which is implied by one node along R coordinate for $\Theta = 0^\circ$. However, certain degree of bending excitation is also clearly present. Figure 5(a) then contains the second state of Σ^+ symmetry (-19.4 cm^{-1}). The state has one nodal plane roughly diagonal in (R, Θ) plane. Hence, there is no clear distinction between stretch and bend excitation in this case. However, this wave function prefers the neon on the side opposite of the hydrogen with $\Theta = 180^\circ$ and thus we can basically interpret this state as a $\text{Ne}-\text{IH}$ isomer. The stretching excitation of this state can be then seen in Fig. 5(b) (-9.7 cm^{-1}). Again the nodal structure is not simple. This state as well as the previous ones of Σ^+ symmetry are far from being separable in R and Θ . The interpretation of the excited states of Π symmetry is more obvious, see Fig. 6. The lowest state of this symmetry (-12.4 cm^{-1}) is simply an almost free HI rotor state with $j=1$ (with $\cos \Phi$ or $\sin \Phi$ dependence) and the corresponding first excited state (-2.3 cm^{-1}) has the same angular dependence but additional stretching excitation in the R coordinate. Unlike for the $\text{Ar}\cdots\text{HI}$ complex,⁵ we cannot interpret these T-shaped states with maxima near $\Theta = 90^\circ$ as bending excitations of certain isomer, such as $\text{Ne}-\text{HI}$ or $\text{Ne}-\text{IH}$.

It is interesting that also states with positive energies are found by imaginary time propagation. These levels correspond to higher states of Π symmetry with total energy above the dissociation threshold of the weakly bound complex. Because of a weak coupling between radial and angular motions these resonances have very long lifetime and should, therefore, be in principle spectroscopically observable. A lower limit of a few nanoseconds for their lifetime was found by real time propagation using Chebyshev expansion of the time evolution operator.⁵⁷

In conclusion of this section, let us briefly summarize possible relations between the minima of the PES and the ground state vibrationally averaged structures. As already noted, complexes of Rg and HX can have two basically collinear structures, either $\text{Rg}-\text{HX}$ or $\text{Rg}-\text{XH}$. Table V repre-

TABLE V. Summary of the three prototypical cases of $\text{Rg}\cdots\text{HX}$ complexes. The table compares energies and structures of minima on the PES with vibrationally averaged structures.

System	Minimum on PES	D_e/cm^{-1}	Structure	D_0/cm^{-1}
$\text{Ne}\cdots\text{HBr}$	$\text{Ne}-\text{HBr}$	-58.6	$\text{Ne}-\text{HBr}$	-29.0
$\text{Ar}\cdots\text{HI}^a$	$\text{Ar}-\text{IH}$	-220.0	$\text{Ar}-\text{IH}$	-146.4
$\text{Ne}\cdots\text{HI}$	$\text{Ne}-\text{IH}$	-55.7	$\text{Ne}-\text{HI}$	-28.3

^aReference 5.

sents three possible situations which can occur in these weakly bound complexes. The first case is the most typical one where both the global minimum on the PES and the vibrationally averaged structure are found at $\Theta=0^\circ$ (Rg–HX). As typical representative of this family of complexes we have discussed $\text{Ne}\cdots\text{HBr}$. The only known case where the situation is exactly opposite is the $\text{Ar}\cdots\text{HI}$ complex.⁵ The third, hitherto unexplored, possibility is the case with the flip of the hydrogen atom upon including the zero point motion, as has been demonstrated in this work on $\text{Ne}\cdots\text{HI}$. A general feature of all these complexes is that zero point motion tends to prefer the Rg–HX structure. This allows us to be confident that even though the difference in the energies of the $\text{Ne}\cdots\text{HBr}$ and $\text{Ne}\cdots\text{BrH}$ minima might be within the accuracy of the *ab initio* method employed, the structure in any case corresponds to the $\text{Ne}\cdots\text{HBr}$ arrangement.

D. Larger clusters: Flip of the hydrogen wave function

As discussed in the previous section, the ground state structures of $\text{Ne}\cdots\text{HBr}$ and $\text{Ne}\cdots\text{HI}$ clusters correspond to hydrogen facing the rare gas atom, despite the fact that the global minimum of $\text{Ne}\cdots\text{HI}$ complex lies at the opposite side. This is in contrast to the ground state structure of the $\text{Ar}\cdots\text{HI}$ complex which corresponds to argon facing directly to the halide (i.e., to the $\text{Ar}\cdots\text{IH}$ arrangement). For this structure, a conclusive experimental evidence has been provided by Wittig *et al.*³⁶ We now address the following question: How does the structure (i.e., the hydrogen wave function) change with increasing number of rare gas atoms in the cluster? This is of a particular interest for the interpretation of experiments concerning photodissociation of HX molecule on the surface of rare gas clusters. After the UV photolysis, systems with hydrogen wave function localized between halogen and rare gas atoms will be characterized by a strong cage effect resulting in a significant peak at low energies in the final hydrogen kinetic energy distribution (KED) spectrum. On the other hand, if the hydrogen initially faces away from the cluster, the cage effect will be negligible.^{29,30,58} In this study we have varied the number of the cage atoms from single argon atom to six argon atoms. The extrapolation to larger clusters is then straightforward, since six argons constitute first solvation half-layer for every larger rare gas cluster with a single substitutional HX impurity on the cluster interface. The interaction potential for larger clusters is constructed from an accurate three body Rg–HX term [for $\text{HI}(\text{Ar})_n$ we have used Bevan's semiempirical potential,⁵ for $\text{HI}(\text{Ne})_n$ and $\text{HBr}(\text{Ne})_n$ systems we have used the present *ab initio* potentials] and from pair potentials for Rg–Rg interactions.⁵⁹ The heavy atom geometries of the $\text{HI}(\text{Ar})_n$, $\text{HBr}(\text{Ne})_n$, and $\text{HI}(\text{Ne})_n$ clusters are similar to those of $\text{HCl}(\text{Ar})_n$ clusters.⁶⁰ Since the hydrogen halide is slightly too large to fit inside the cluster, it prefers the surface position even for large rare gas clusters. The symmetries of optimal structures, as obtained by potential minimization, are C_{2v} for $\text{HX}(\text{Ar})_2$ system, C_{3v} for $\text{HX}(\text{Ar})_3$, C_{2v} for $\text{HX}(\text{Ar})_4$, C_{4v} for $\text{HX}(\text{Ar})_5$, and C_{5v} for $\text{HX}(\text{Ar})_6$.

The librational wave functions for $\text{HBr}(\text{Ne})_n$ clusters are depicted in Fig. 7. The character of the ground librational

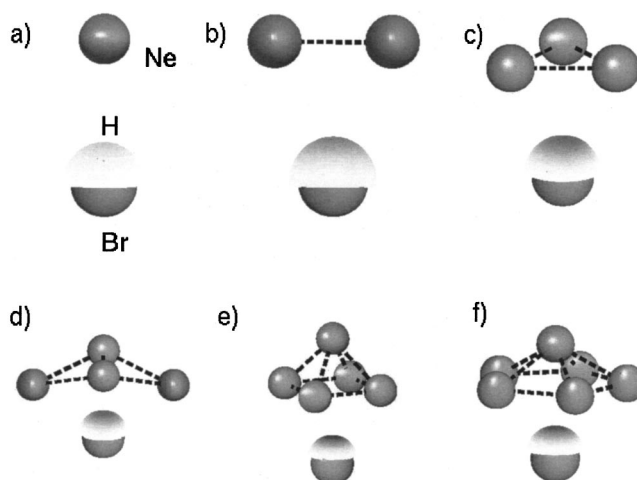


FIG. 7. Size dependence of the ground vibrational (librational) wave function for HBr on Ne_n ($n=1-6$). Note that in all cases the hydrogen atom points towards the rare gas clusters.

state does not change dramatically upon increasing cluster size for the $\text{HBr}(\text{Ne})_n$ and $\text{HI}(\text{Ne})_n$ clusters. Starting from a single rare gas solvent atom, the hydrogen wave function is pointing towards the cluster. Therefore, after photodissociation, one can expect a significant cage effect, and consequently, the shift to smaller values in the kinetic energy distribution of the H fragment.

The situation for $\text{HI}(\text{Ar})_n$ clusters is more complicated and interesting at the same time. The hydrogen wave functions for this complex are depicted in Fig. 8. The ground state of the smallest cluster with a single rare gas atom is associated with the $\text{Ar}\cdots\text{IH}$ geometry. Also in the $\text{HI}(\text{Ar})_2$ complex hydrogen points away from the rare gas atoms. The crucial point is that for $\text{HI}(\text{Ar})_3$ the librational wave function flips and the hydrogen now points towards the argons. For $\text{HI}(\text{Ar})_4$ hydrogen flips back and the situation is similar to $\text{HI}(\text{Ar})_2$, since HI interacts effectively only with the two closer argon atoms. Starting from the $\text{HI}(\text{Ar})_5$ cluster the optimal vibrationally averaged structure corresponds again to the $\text{IH}\cdots\text{Rg}_n$ geometry. In conclusion, although hydrogen

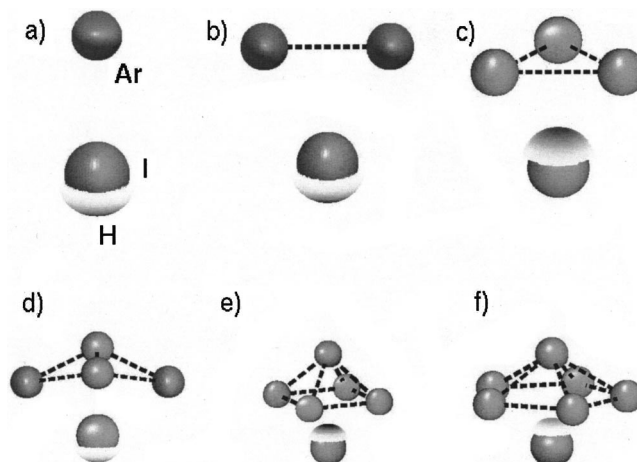


FIG. 8. Size dependence of the ground vibrational (librational) wave function for HI on Ar_n ($n=1-6$). Note the flip of the H wave function towards the rare gas clusters upon increasing cluster size.

points away from the complex for the $\text{HI}(\text{Ar})_n$ ($n = 1, 2,$ and 4) clusters, starting from five argon surface solvated HI always has hydrogen pointing towards the rare gas atoms.

There is a nice piece of experimental evidence supporting the present calculated size evolution of the hydrogen wave function in $\text{HI}(\text{Ar})_n$ clusters based on comparison of the measurements of Wittig *et al.*³⁶ and the experiments of Baumfalk and Buck.^{31,32} Wittig reported the photodissociation of the $\text{Ar} \cdots \text{HI}$ complex, where no caging was detected (the H kinetic energy distribution was actually shifted to slightly higher energies), while Baumfalk and Buck studied large argon clusters (approximately 100 argon atoms) with HI on the surface and significant caging was observed. In future, it would be interesting to explore the predicted flip of the the hydrogen wave function in more detail. In particular, an experimental study of $\text{HI}(\text{Ar})_2$ and $\text{HI}(\text{Ar})_3$ should bring new insight into the intriguing quantum behavior of these systems.

V. CONCLUSIONS

The main points addressed in the present paper can be summarized as follows:

- (1) We have calculated using the CCSD(T) *ab initio* method accurate potential energy surfaces of $\text{Ne} \cdots \text{HBr}$ and $\text{Ne} \cdots \text{HI}$;
- (2) We have constructed intermolecular vibrational states of $\text{Ne} \cdots \text{HBr}$, $\text{Ne} \cdots \text{HI}$, and $\text{HI}(\text{Ar})_n$ ($n = 1-6$);
- (3) We have shown that for cryogenic complexes containing hydrogen moving in a shallow bending potential a correct description should be based on vibrationally averaged structures rather than on minima on the potential energy surfaces;
- (4) We have demonstrated that for the $\text{Ne} \cdots \text{HI}$ cluster the global minimum corresponds to the $\text{Ne}-\text{IH}$ geometry, however, the optimal vibrationally averaged structure has hydrogen between the heavy atoms;
- (5) We have interpreted seemingly conflicting experimental data on $\text{HI} \cdots \text{Ar}$ and large $\text{HI}(\text{Ar})_n$ clusters in terms of a flip of the hydrogen towards the rare gas atoms upon increasing the number of argons.

In summary, the main goal has been to demonstrate the importance of quantum delocalization, in particular that connected with the large amplitude hydrogen bending motion, in cryogenic $\text{Rg} \cdots \text{HX}$ clusters. As a matter of fact, the vibrational quantum effect can become more important for determining the energetically lowest isomeric structure than the relative depths of the minima on the PES.

ACKNOWLEDGMENTS

We are grateful to R. R. Lucchese for providing us their $\text{Ar} \cdots \text{HI}$ potential and to K. Faegri for sending us his basis set. This work has been supported by the Volkswagen foundation via Grant No. I/75908. Support of the Czech Ministry of Education to the Center for Complex Molecular Systems and Biomolecules (Grant No. LN00A032) is gratefully acknowledged.

- ¹K. R. Leopold, G. T. Fraser, S. E. Novick, and W. Klemperer, *Chem. Rev.* **94**, 1807 (1994).
- ²R. L. Robinson, D.-H. Gwo, and R. J. Saykally, *J. Chem. Phys.* **87**, 5149 (1987).
- ³M. R. Keenan, E. J. Campbell, T. J. Balle, L. W. Buxton, T. K. Minton, P. D. Soper, and W. H. Flygare, *J. Chem. Phys.* **72**, 3070 (1980).
- ⁴D. W. Firth, M. A. Dvorak, S. W. Reeve, R. S. Ford, and K. R. Leopold, *Chem. Phys. Lett.* **168**, 161 (1990).
- ⁵A. McIntosh, Z. Wang, J. Castillo-Chará, R. R. Lucchese, J. W. Bevan, R. D. Suenram, and A. C. Legon, *J. Chem. Phys.* **111**, 5764 (1999).
- ⁶J. Han, A. L. McIntosh, Z. Wang, R. R. Lucchese, and J. W. Bevan, *Chem. Phys. Lett.* **265**, 209 (1997).
- ⁷J. M. Hutson, *J. Chem. Phys.* **89**, 4550 (1988).
- ⁸J. M. Hutson, *J. Phys. Chem.* **96**, 4237 (1992).
- ⁹J. M. Hutson, *J. Chem. Phys.* **96**, 6752 (1992).
- ¹⁰M. Meuwly and J. M. Hutson, *J. Chem. Phys.* **110**, 8338 (1999).
- ¹¹J. M. Hutson, *J. Chem. Phys.* **91**, 4448 (1989).
- ¹²J. M. Hutson, *J. Chem. Phys.* **91**, 4455 (1989).
- ¹³P. Niyaz, Z. Bacic, J. W. Moskowitz, and K. E. Schmidt, *Chem. Phys. Lett.* **252**, 23 (1996).
- ¹⁴C. E. Dykstra, *J. Chem. Phys.* **108**, 6619 (1998).
- ¹⁵M. Lewerenz, *J. Chem. Phys.* **104**, 1028 (1996).
- ¹⁶J. Franck and E. Rabinowitch, *Trans. Faraday Soc.* **30**, 120 (1934).
- ¹⁷A. Garcia-Vela, *J. Chem. Phys.* **108**, 5755 (1998).
- ¹⁸T. Schroeder, R. Schinke, M. Mandziuk, and Z. Bacic, *J. Chem. Phys.* **100**, 7239 (1994).
- ¹⁹E. Narevicius, D. Neuhauser, H. J. Korsch, and N. Moiseyev, *Chem. Phys. Lett.* **276**, 250 (1997).
- ²⁰M. Monnerville and B. Pouilly, *Chem. Phys. Lett.* **294**, 473 (1998).
- ²¹A. Garcia-Vela, R. B. Gerber, and U. Buck, *J. Phys. Chem.* **98**, 3518 (1994).
- ²²R. Alimi and R. B. Gerber, *Phys. Rev. Lett.* **64**, 1453 (1990).
- ²³M. Niv, A. I. Krylov, and R. B. Gerber, *Faraday Discuss. Chem. Soc.* **108**, 243 (1997).
- ²⁴M. Niv, A. I. Krylov, R. B. Gerber, and U. Buck, *J. Chem. Phys.* **1110**, 11047 (1999).
- ²⁵R. Baumfalk, N. H. Nahler, U. Buck, M. Y. Niv, and R. B. Gerber, *J. Chem. Phys.* **113**, 329 (2000).
- ²⁶B. Schmidt, P. Jungwirth, and R. B. Gerber, in *Ultrafast Chemical and Physical Processes in Molecular Systems*, edited by M. Chergui (World Scientific, Singapore, 1996), p. 637.
- ²⁷J. Manz, P. Saalfrank, and B. Schmidt, *J. Chem. Soc., Faraday Trans.* **93**, 957 (1997).
- ²⁸B. Schmidt, *Chem. Phys. Lett.* **301**, 207 (1999).
- ²⁹P. Zdanska, B. Schmidt, and P. Jungwirth, *J. Chem. Phys.* **110**, 6246 (1999).
- ³⁰P. Zdanska, P. Slavicek, and P. Jungwirth, *J. Chem. Phys.* **112**, 10761 (2000).
- ³¹R. Baumfalk, Ph.D. thesis, Göttingen, 1999.
- ³²R. Baumfalk and U. Buck, *Faraday Discuss. Chem. Soc.* (in press).
- ³³T. A. Beu, U. Buck, I. Ettischer, M. Hobein, J. G. Siebers, and R. J. Wheatley, *J. Chem. Phys.* **106**, 6806 (1997).
- ³⁴D. C. Clary, D. M. Benoit, and T. V. Mourik, *Acc. Chem. Res.* **33**, 441 (2000).
- ³⁵K. Liu, M. G. Brown, C. Carter, R. J. Saykally, J. K. Gregory, and D. C. Clary, *Nature (London)* **381**, 501 (1996).
- ³⁶C. Jaques, L. Valachovic, S. Ionov, E. Böhmer, Y. Wen, J. Segall, and C. Wittig, *J. Chem. Soc., Faraday Trans.* **89**, 1419 (1993).
- ³⁷S. F. Boys and F. Bernardi, *Mol. Phys.* **19**, 553 (1970).
- ³⁸<http://www.emsl.pnl.gov:2080/forms/basisform.html>
- ³⁹D. E. Woon and T. H. Dunning, Jr., *J. Chem. Phys.* **98**, 1358 (1993).
- ⁴⁰A. K. Wilson, D. E. Woon, K. A. Peterson, and T. H. Dunning, Jr., *J. Chem. Phys.* **110**, 7667 (1999).
- ⁴¹T. H. Dunning, Jr., *J. Chem. Phys.* **90**, 1007 (1989).
- ⁴²P. O. Widmark, B. J. Persson, and B. Roos, *Theor. Chim. Acta* **79**, 419 (1991).
- ⁴³G. Chałasiński, M. M. Szczęśniak, and B. Kukawska-Tarnawska, *J. Chem. Phys.* **94**, 6677 (1991).
- ⁴⁴L. A. LaJohn, P. A. Christiansen, R. B. Ross, T. Atashroo, and W. C. Ermler, *J. Chem. Phys.* **87**, 2812 (1987).
- ⁴⁵L. Visscher and K. G. Dyall, *J. Chem. Phys.* **104**, 9040 (1996).
- ⁴⁶L. Visscher, J. Styszyński, and W. C. Nieuwpoort, *J. Chem. Phys.* **105**, 1987 (1996); K. Faegri (private communication).

- ⁴⁷J. V. Burda, P. Hobza, and R. Zahradník, *Chem. Phys. Lett.* **288**, 20 (1998).
- ⁴⁸F.-M. Tao and Y.-K. Pan, *Chem. Phys. Lett.* **194**, 162 (1992); *J. Chem. Phys.* **97**, 4989 (1992).
- ⁴⁹F.-M. Tao and W. Klemperer, *J. Chem. Phys.* **101**, 1129 (1994).
- ⁵⁰R. Burcl, G. Chałasiński, R. Bukowski, and M. M. Szczęśniak, *J. Chem. Phys.* **103**, 1498 (1995).
- ⁵¹H. L. Williams, E. M. Mas, K. Szalewicz, and B. Jeziorksi, *J. Chem. Phys.* **103**, 7374 (1995).
- ⁵²M. J. Frisch, G. W. Trucks, H. B. Schlegel *et al.*, GAUSSIAN98 (Gaussian, Inc., Pittsburgh, PA, 1998).
- ⁵³R. Kosloff and H. Tal-Ezer, *Chem. Phys. Lett.* **127**, 223 (1986).
- ⁵⁴T. Suzuki, H. Katayanagi, and M. C. Heaven, *J. Phys. Chem.* **101**, 6697 (1997).
- ⁵⁵A. Bagno, *J. Chem. Soc., Faraday Trans.* **94**, 2501 (1998).
- ⁵⁶G. Herzberg, *Molecular Spectra and Molecular Structure* (Van Nostrand, New York, 1950).
- ⁵⁷R. Kosloff, *J. Phys. Chem.* **92**, 2087 (1988).
- ⁵⁸P. Slavicek, P. Zdanska, P. Jungwirth, R. Baumfalk, and U. Buck, *J. Phys. Chem. A* **104**, 7793 (2000).
- ⁵⁹R. A. Aziz and M. J. Slaman, *Mol. Phys.* **58**, 679 (1986).
- ⁶⁰D. T. Anderson, S. Davis, and D. J. Nesbitt, *J. Chem. Phys.* **107**, 1115 (1997).